The Nature of Excited-State Absorption in Polymethine and Squarylium Molecules

Raluca A. Negres, Olga V. Przhonska, David J. Hagan, *Senior Member, IEEE*, Eric W. Van Stryland, Mikhail V. Bondar, Yuriy L. Slominsky, and Alexei D. Kachkovski

***Abstract*—Subpicosecond transient absorption measurements were performed for several polymethine and squarylium dyes in ethanol solution and a polymeric host over the spectral range 400–1500 nm. A variety of nonlinear effects including saturable absorption, reverse saturable absorption, and gain were observed and analyzed. We observe strong excited-state absorption (ESA) in all dyes in the range 450–600 nm. We also report the first prediction and observation of additional ESA bands in the near-infrared range. The predictions were based on quantum chemical calculations and the ESA experiments were performed with femtosecond pump-continuum probe techniques. For polymethine dye 2-[2-[3-[(1,3-dihydro-3,3-dimethyl-1-phenyl-2H-indol-2-ylidene) ethylidene]-2-phenyl-1-cyclohexen-1-yl]ethenyl]-3,3-dimethyl-1-phenylindolium perchorate, an additional ESA band was detected near 1250 nm, and for squarylium dye 1,3-Bis-[(1,3-dihydro-1-butyl-3,3-dimetyl-2H-benzo[e]indol-2-ylidene)methyl]squaraine, two additional ESA bands were found around 870- and 1380-nm, respectively. To further study the nature of these transitions, the steady-state excitation anisotropy was also studied and compared with predictions. The relationship between ESA spectra of organic dyes and their molecular structure is discussed.**

***Index Terms*—Excited state absorption, femtosecond, nonlinear optics, nonlinear spectroscopy, polymethine dyes, quantum chemical calculations, white-light continuum.**

I. Introduction

POLYMETHINE (PD) and squarylium (SD) dyes have been extensively studied as promising compounds for laser and photonics technologies. These dyes offer the possibility of systematic modification of their structure using different heterocyclic terminal groups, introducing specific substituents into the polymethine chain, branching of the polymethine chromophore, and cyclization of the chain by conjugated or unconjugated bridges. Many correlations between the molecular structure of PDs and their linear optical parameters, such as the position of absorption and emission spectra, Stokes shift, fluorescence quantum yield, probability of trans-cis isomerization, and photochemical stability, have already been established [1]. Currently, semi-empirical computational methods [Austin Model 1 (AM1) for geometries and ZINDO for electronic transition energies] have been developed to calculate the charge distribution in the ground (S_0), first (S_1), and higher excited states (S_i), transition energy $S_0 \rightarrow S_i$ [2], [3], ground and excited-state potential energy surfaces [4], barriers of photoisomerization [5], etc. Understanding the relationships between molecular structure and nonlinear optical parameters of organic dyes could provide the guideline to optimization and synthesis of new molecules with improved properties for nonlinear optical applications. A detailed theoretical investigation of molecular polarizabilities and hyperpolarizabilities as a function of molecular structure is given in [6]. Correlations between molecular structure and nonlinear properties, such as photoinduced excited-state absorption, excited-state molecular dynamics, and anisotropy of nonlinear response, are much less investigated. Reliable quantum-chemical calculations for transitions from the first excited state to higher levels, $S_1 \rightarrow S_i$, require systematical calibration and comparison with the experimental excited-state absorption (ESA) bands. To our knowledge, this analysis for polymethine and squarylium dyes has yet to be performed in more detail. Experimental investigations are therefore the most valuable tools for both advancing theoretical understanding and further development and optimization of organic molecules for practical applications. Currently, [7] and [8] provide the most extensive experimental information about the transient absorption of PDs in a wide spectral range 350–1000 nm.

In this paper, we describe experimental and theoretical studies of PD and SD molecules that aid in the understanding of:

1) the nature of the transitions from the ground state and from the first excited state into the higher excited states, i.e., $S_0 \rightarrow S_i$ and $S_1 \rightarrow S_i$;
2) what molecular fragments are responsible for these transitions.

The experimental techniques used to investigate these molecules are:

1) Z-scan;
2) femtosecond pump-probe;
3) steady-state excitation anisotropy measurement;
4) linear absorption spectra measurement.

The analysis techniques include:

1) quantum-chemical calculations using Austin Model 1 (HyperChem software package) and Parr–Pariser–Pople approximations;

Manuscript received May 14, 2001; revised August 2, 2001. This work was supported by the National Science Foundation under Grant ECS 9970078, by the Office of Naval Research under Grant N00014-97-1-0936, and by the Naval Air Warfare Center Joint Service Agile Program under Contract N00421-98-C-1327.

R. A. Negres, D. J. Hagan, and E. W. Van Stryland are with the School of Optics/Center for Research and Education in Optics and Lasers, University of Central Florida, Orlando, FL 32816-2700 USA.

O. V. Przhonska is with the School of Optics/Center for Research and Education in Optics and Lasers, University of Central Florida, Orlando, FL 32816-2700 USA and the Institute of Physics, National Academy of Sciences of Ukraine, 03028 Kiev-28, Ukraine.

M. V. Bondar is with the Institute of Physics, National Academy of Sciences of Ukraine, 03028 Kiev-28, Ukraine.

Y. L. Slominsky and A. D. Kachkovski are with the Institute of Organic Chemistry, National Academy of Sciences of Ukraine, 02094 Kiev-94, Ukraine.

Publisher Item Identifier S 1077-260X(01)11222-0.

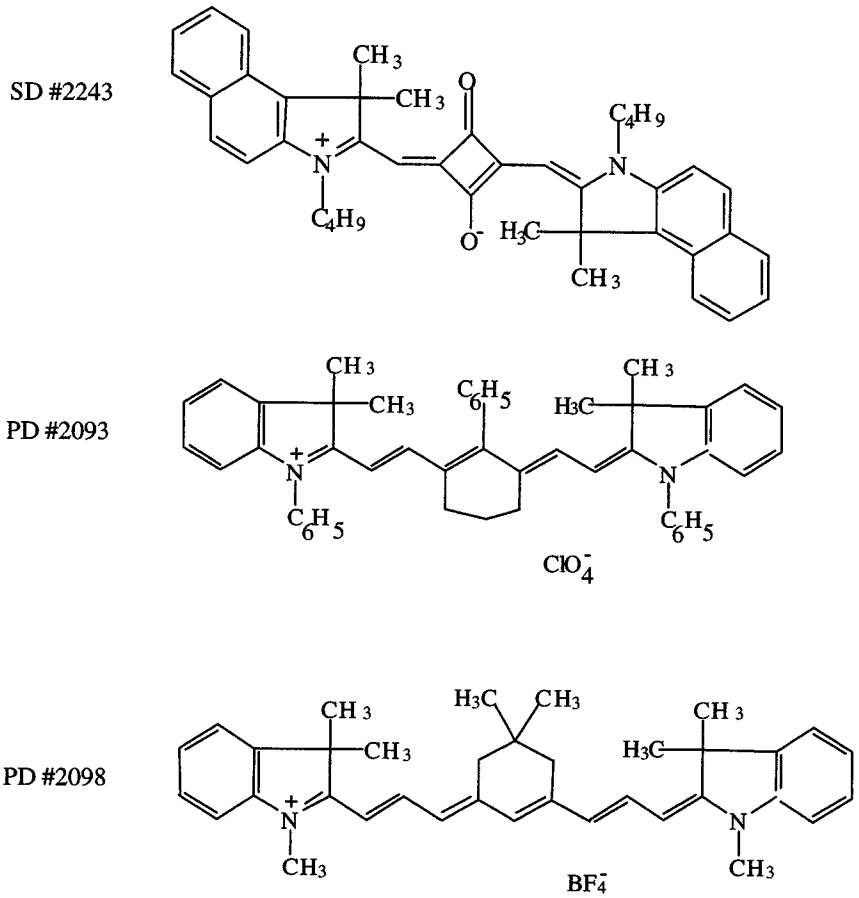

Fig. 1. Molecular structures of dyes.

2) numerical fitting of the Z-scan data.

In the next section, we describe the main properties of the dyes under investigation and quantum-chemical methods.

II. Materials and Quantum-Chemical Methods

A. Materials

The molecular structures of the dyes studied, 2-[2-[3-[(1,3-dihydro-3,3-dimethyl-1-phenyl-2H-indol-2-ylidene)ethylidene]-2-phenyl-1-cyclohexen-1-yl]ethenyl]-3,3-dimethyl-1-phenylindolium perchorate, labeled as PD #2093, 2-[2-[3-[(1,3-dihydro-3,3-dimethyl-1-phenyl-2H-indol-2-ylidene)ethylidene]-4-methyl-2-(4-methoxyphenyl)-1-cyclohexen-1-yl]ethenyl]-3,3-dimethyl-1-phenylindolium tetrafluoroborate, labeled as #2303; 2-[3-[3-[(1,3-dihydro-1,3,3-trimethyl-2H-indol-2-ylidene)-1-propen-1-yl]-5,5-dimethyl-2-cyclohexen-1-ylidene]-1-propen-1-yl]-1,3,3-trimethylindolium tetrafluoroborate, labeled as #2098; and squarylium dye, 1,3-Bis-[(1,3-dihydro-1-butyl-3,3-dimetyl-2H-benzo[e]indol-2-ylidene)methyl]squaraine, labeled as SD #2243, are shown in Fig. 1. These dyes were synthesized at the Institute of Organic Chemistry, Kiev, Ukraine. Their molecular structures were confirmed by elemental analysis and nuclear magnetic resonance spectra. These particular dyes were chosen based on their photophysical and nonlinear optical properties, particularly their reverse saturable absorption (RSA) properties, which are favorable for passive optical limiting. As was found in our previous paper [9], PD #2093 (this dye is labeled "PD3" in [9]) exhibits strong RSA and is photochemically stable. In [9], the excited-state and ground-state absorption cross-sections for this dye in ethanol at a wavelength of 532 nm were reported as $\sigma_{1i}(532) = 3 \times 10^{-16}$ cm^2 and $\sigma_{01}(532) = 1.5 \times 10^{-18}$ cm^2, respectively. Both of these numbers are large, as are their ratios, which are requirements for efficient optical limiting [10].

The experiments were performed in two host media: absolute ethanol and an elastopolymer of polyurethane acrylate (PUA). The polymeric samples were prepared by a previously reported radical photopolymerization procedure [9], [11]. The room-temperature linear absorption spectra presented in Fig. 2 were recorded with a Varian Cary 500 spectrophotometer.

The spectroscopic and nonlinear optical properties of PDs are determined primarily by the existence of the delocalized π-electron systems in the polymethine chromophore and symmetric terminal groups. Inclusion of a six-link cycle with phenyl substituent into the polymethine chromophore for PD #2093 and a six-link cycle with a more complicated acceptor substituent for PD #2303 shifts their absorption maxima by 32 and 28 meV, respectively, to the red region compared with their unsubstituted analog (258 and 224 cm^{-1}). The linear absorption maximum is at 770 nm for PD #2093 and at 768 nm for PD #2303 in ethanol solution. PD #2098 is characterized by a lengthening of the

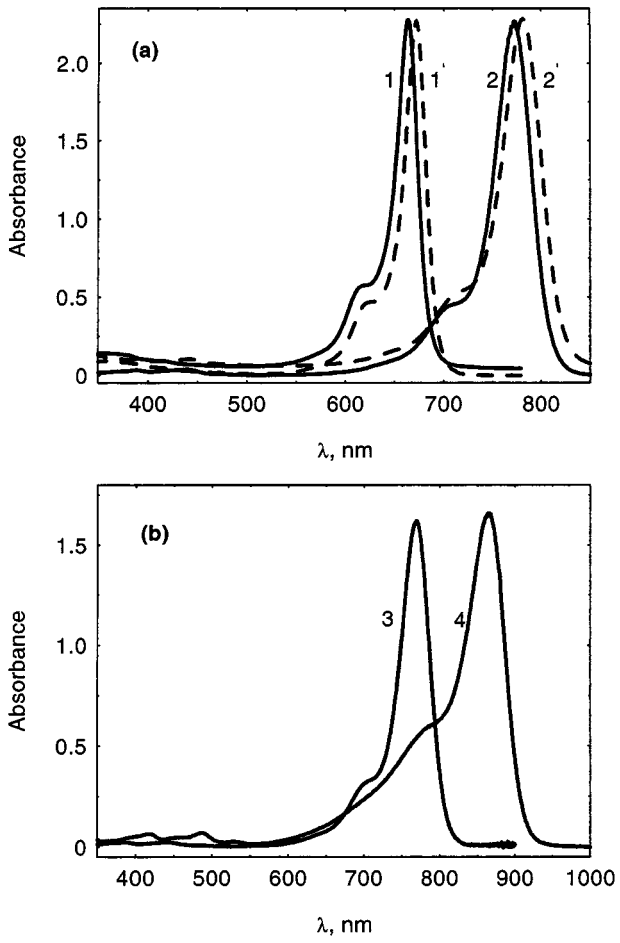

Fig. 2. (a) Linear absorption spectra of SD #2243 (1, 1') and PD #2093 (2, 2') in ethanol (solid lines 1 and 2) and PUA (dashed lines 1' and 2'). (b) Linear absorption spectra of PD #2303 (3) and PD #2098 (4) in ethanol.

polymethine chromophore due to the introduction of an additional methine (CH=CH) group. Therefore, its absorption maximum is red-shifted by 176 meV compared to PD #2093 (1413 cm^{-1}). Its polymethine chromophore is also partly strengthened by the unconjugated bridge. The linear absorption maximum for PD #2098 is placed at 864 nm in ethanol and 877 nm in PUA.

The main distinguishing features of SD #2243 are the existence of the central "square" group C_4O_2 and the long C_4H_9 butyl tails connected to nitrogen atoms at the end of the chromophore. In contrast to the PDs, squarylium dyes are neutral with the localization of the positive charge on the nitrogen atom and the negative charge on the oxygen atom of the central group as followed from quantum-chemical calculations. Most SDs are characterized by large extinction coefficients and narrow absorption bands associated with the $S_0 \rightarrow S_1$ transition. The long butyl tails improve the solubility of the dye in both ethanol and PUA and prevent the formation of aggregates even at large concentrations of the dye up to (1.5–2) $\times 10^{-3}$ M/l. The linear absorption maximum for SD #2243 is at 663 nm in ethanol and 672 nm in PUA.

B. Quantum-Chemical Calculations

The optimized geometry of the dye molecules as well as the electron transition energies and oscillator strengths were obtained using the HyperChem software package under the AM1 approximation. The excited state wave functions were represented as an expansion of 60 single excited configurations. Also, the electron transition characteristics (energies and electron density redistribution upon excitation) were calculated in the Parr–Pariser–Pople (PPP) approximation with the same optimized geometry, as modified by Fabian and Zahradnic for linear conjugated systems [12]. In this paper, we do not go beyond these simplest methods, which proved themselves as a reliable technique to analyze the nature of the $\pi \rightarrow \pi^*$ transitions in such multielectron systems as polymethine and squarylium dyes [13]. The known semi-empirical methods AM1 and PPP are mainly parameterized for calculation of the lowest electron transitions. Nevertheless, as we shall show, there is a comparatively good correlation between the calculated and experimental energies for some higher transitions $S_0 \rightarrow S_i$. In this paper, the standard AM1 and PPP methods are used, without any additional assumptions, for calculations of the $S_1 \rightarrow S_i$ transitions, so these energies are obtained by the subtractions $\Delta E(S_1 \rightarrow S_i) = \Delta E(S_0 \rightarrow S_i) - \Delta E(S_0 \rightarrow S_1)$.

III. Experiment

A. Methods

1) Z-Scan Measurements of ESA at 532 nm: To determine the excited-state cross-sections at 532 nm, we used the open-aperture Z-scan technique [9]–[11]. For these experiments, 30-ps full-width at half-maximum (FWHM) pulses at 532 nm were produced by generating the second harmonic of a Q-switched and mode-locked Nd : YAG laser operating at a 10-Hz repetition rate with single pulses switched out of the mode-locked train. These were focused by a 10-cm focal-length lens to a beam waist of 22 μm HW1/e^{2}M. Tthe total transmitted energy was monitored as the samples were scanned along the beam axis from one side of the focal plane to the other. At this wavelength, the linear absorption corresponds to an excitation into the short wavelength tail of the main absorption bands for PD #2303, PD #2093, and SD #2243 and into the second absorption band $S_0 \rightarrow S_2$ for PD #2098. A simplified level structure for these dyes is presented in Fig. 3. From linear transmittance measurements, ground-state absorption cross-sections at 532 nm in ethanol were determined as σ_{01}(SD #2243) $= 1.7 \times 10^{-18}$ cm^2; σ_{01}(PD #2303) $= 2.3 \times 10^{-18}$ cm^2; and σ_{02}(PD #2098) $= 1.5 \times 10^{-17}$ cm^2. All of these dyes show RSA, which indicates that σ_{01}(532 nm) $\ll \sigma_{1i}$(532 nm). Numerical fitting of the Z-scan data was performed using a three-level model $S_0 \rightarrow S_1 \rightarrow S_i$ (all singlet states), which adequately explains our picosecond results [9]. From this fitting procedure, we find σ_{1i}(SD #2243) $= 2.5 \times 10^{-16}$ cm^2; σ_{1i}(PD #2303) $= 4.3 \times 10^{-16}$ cm^2, and σ_{1i}(PD #2098) $= 3.8 \times 10^{-16}$ cm^2. Thus all of these dyes are characterized by extremely large excited-state absorption in the visible region. The ratios of σ_{1i}/σ_{01} on 532 nm for ethanol solution are approximately 150 for SD #2243, 190 for PD #2303, 25 for PD #2098, and 200 for PD #2093. The smallest ratio obtained for PD #2098 is explained by the high linear ($S_0 \rightarrow S_2$) absorption at 532 nm compared to the other dyes ($S_0 \rightarrow S_1$).

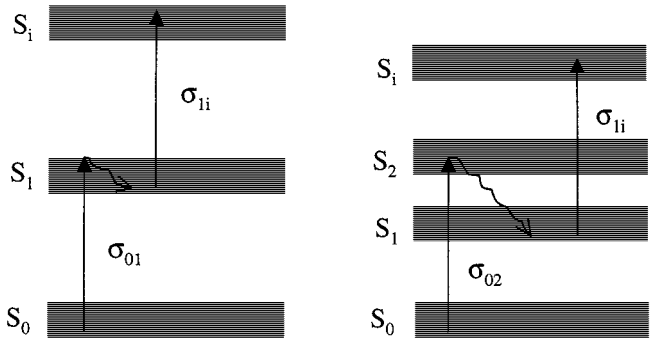

Fig. 3. Simplified energy-level structure of dyes.

2) Fluorescence Excitation Anisotropy Measurements: Steady-state fluorescence spectra (using low-concentration $\sim 10^{-6}$ M/l liquid dye solutions to avoid reabsorption) as well as anisotropy excitation spectra were obtained with an SLM 8000 Spectrofluorimeter for PD #2093 and a PTI Quantamaster Spectrofluorimeter for SD # 2243. To understand the nature of the $S_0 \rightarrow S_i$ transitions, the anisotropy excitation spectra $R(\lambda)$ were calculated as a function of the excitation wavelength λ at fixed emission wavelength after appropriate blank subtraction on each component when needed. $R(\lambda)$ is defined as

$$R(\lambda) = \frac{I_{vv}(\lambda) - G(\lambda) I_{vh}(\lambda)}{I_{vv}(\lambda) + 2G(\lambda) I_{vh}(\lambda)} \tag{1}$$

where $G(\lambda) = I_{hv}(\lambda)/I_{hh}(\lambda)$ and $I_{vv}(\lambda)$, $I_{hv}(\lambda)$, $I_{vh}(\lambda)$, and $I_{hh}(\lambda)$ are the polarized fluorescence intensities at the excitation wavelength λ. The first and second subscripts refer to the orientation (v for vertical and h for horizontal) of the emission and excitation polarizations, respectively [14]. The results of steady-state excitation anisotropy measurements are presented below.

3) Measurements of Nonlinear Absorption Spectra: To determine the spectrum of excited-state absorption, transient absorption in PDs and SD #2243 was measured by a pump-probe method where the probe is a subpicosecond white-light continuum (WLC) [15]. Femtosecond pulses ($\lambda = 775$ nm, FWHM $= 150$ fs, 1 kHz repetition rate, 900 μJ/pulse) from a regeneratively amplified laser source (Clark-MXR, Inc., model CPA-2001) are split to pump two optical parametric generator/amplifier (OPG/OPA) systems (Light Conversion Ltd., model TOPAS). Output pulses have energies of tens of microjoules in the wavelength range 500 to 2200 nm. This range is achieved either directly from the OPA or by mixing of the signal, idler, and pump wavelengths. One OPA is set at 670 nm, in the absorption band of both PDs and SD #2243, and the second OPA could be tuned through the infrared (IR) region, where it was either used as a tunable probe or focused tightly into sapphire to generate a WLC.

The experimental setup is shown schematically in Fig. 4. The WLC is produced by focusing 1–2 μJ energy pulse at a wavelength of 2.2 μm (idler) radiation from OPA-1 into a 1-mm sapphire window. The spectrum of the WLC thus obtained covers the range from 450 nm to $>$1700 nm. Two lenses are used to image the WLC probe beam onto the sample. The WLC transmitted by the sample is then imaged onto the fiber input to a 1/4 m spectrometer coupled to a Si or InGaAs dual photodiode array. The Si array provides a wavelength range of 400–1000 nm, while the InGaAs array extends the range out to 1700 nm. The pump beam is attenuated using a polarization rotator [16] followed by a Glan polarizer. No focusing lens is necessary in the pump path, due to the large linear absorption of these dyes at 670 nm. The large spatial extent of the pump beam also ensures a uniform excitation fluence seen by the probe beam inside the sample. The two beams can be time delayed with respect to each other to measure excited-state and reorientational lifetimes, but for these measurements we are primarily interested in the excited-state absorption spectrum. Therefore, we used a fixed 80-ps time delay of the probe beam, which is much greater than the vibrational relaxation times, but much less than the decay time of the excited-state population (as determined previously in [9]). Since the theoretical calculations predicted additional ESA in the near IR region, which was expected to be much weaker than in the visible, the experimental setup was slightly modified to a narrow-band probe arrangement for a better signal-to-noise ratio detection. In the region 700–1000 nm, narrow-band filters (NBFs) were used to select a 10-nm probe bandwidth from the WLC. For longer wavelength regions, since NBF filters were unavailable, we used the direct output from OPA-2, tuned from 1160 to 1600 nm in 20-nm steps. For these single-wavelength probe experiments, large-area photodiodes (Si and Ge) replaced the fiber input spectrometer to measure the probe transmittance.

B. Results

1) Excitation Anisotropy Measurements and Absorption $S_0 \rightarrow S_i$: It is well known that the absorption spectra in the visible and near-IR region for PDs and SDs are characterized by a strong single band $S_0 \rightarrow S_1$ with a typical FWHM $=$ (650–880) cm^{-1}; see Fig. 2(a) and (b). A small vibrational maximum due to carbon–carbon deformational vibrations is situated about 1200 cm^{-1} above the main IR peak. The absorption spectra in the short wavelength region are characterized by small intensity and strongly overlapped bands, which correspond to transitions from the ground to the higher excited states. To distinguish between different $S_0 \rightarrow S_i (i = 2, 3 \cdots)$ transitions, we performed anisotropy excitation measurements. In these measurements, the fluorescence intensity at 820 nm resolved into components parallel to (I_{II}) and perpendicular to ($I_{\perp}$); the excitation polarization was measured as a function of excitation wavelength. By plotting the fluorescence anisotropy R, defined as $R = (I_{||} - I_{\perp})/(I_{||} + 2I_{\perp})$, versus the excitation wavelength, we obtain the anisotropy excitation spectrum [13]. The steady-state anisotropy excitation spectra for PD #2093 and SD #2243 in glycerol are presented in Fig. 5(a) and (b). Measurements in ethanol show the same positions in anisotropy peaks but with smaller anisotropy values (maximum 0.06–0.07). In high-viscosity glycerol solutions, the rate of reorientational motions in the excited state is much slower, and anisotropy values within the first absorption band are high and close to the theoretical limit, 0.3–0.4 [14].

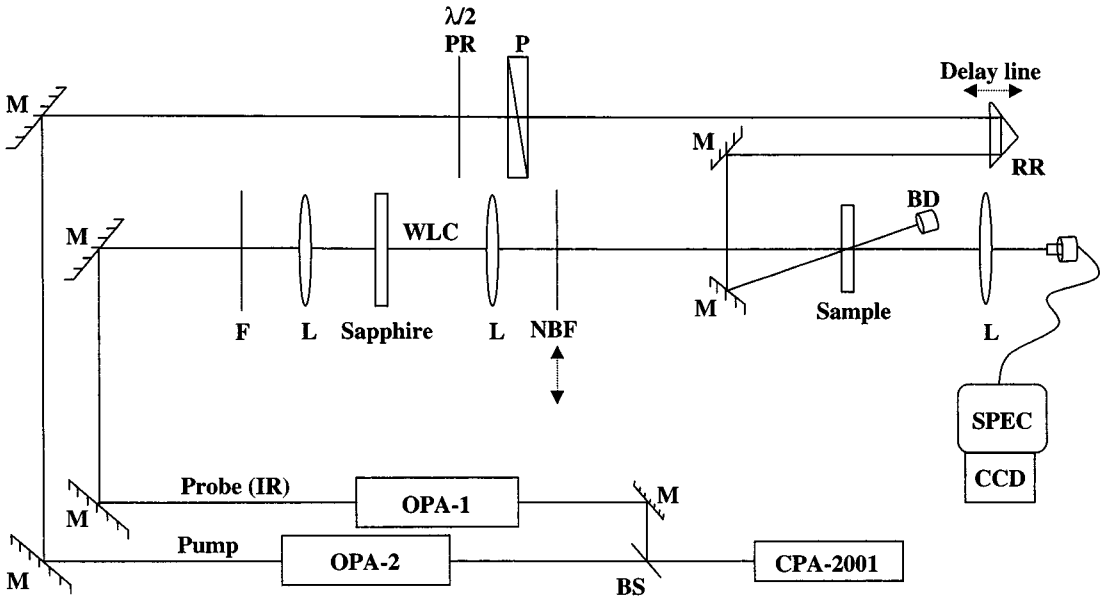

Fig. 4. Schematic of apparatus for measurement of excited state absorption spectra. BS-60/40 beamsplitter, M: mirror, $\lambda/2$ PR: polarization rotator, P: polarizer, RR: retro-reflector, BD: beam dump, L: lens, F: neutral density filter, NBF: narrow-band filter, SPEC: fiber input spectrometer, CCD: CCD dual diode array for spectrum visualization.

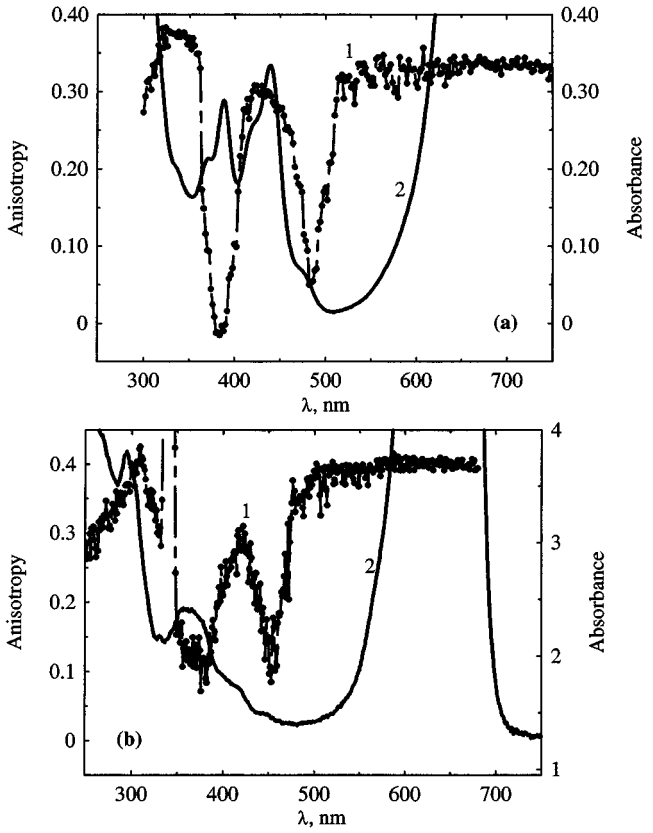

Fig. 5. (a) Anisotropy (1) in glycerol and linear absorption spectrum (right axis y) for PD # 2093 in ethanol (2). Fluorescence (λ registration) was fixed at 820 nm. (b) Anisotropy (1) in glycerol and linear absorption spectra (right axis y) for SD #2243 in ethanol (2). Fluorescence (λ registration) was fixed at 680 nm. The peak at 340 nm is the scattering line corresponding to second harmonic of λ registration.

As can be seen from Fig. 5, the anisotropy values are high and constant over the first excited state $S_0 \rightarrow S_1$ and exhibit a significant drop over the second band $S_0 \rightarrow S_2$, which is placed around 480 nm for PD #2093 and 455 nm for SD #2243. This indicates that the absorption dipole moment of the second transition is oriented at a significant angle to that of the first transition. The next increase in the anisotropy value up to 0.28–0.3 for both dyes reveals the position of the $S_0 \rightarrow S_3$ transition (420 nm for SD #2243 and 430 nm for PD #2093) and parallel orientation of the dipole moment to the $S_0 \rightarrow S_1$ transition. The next drop in anisotropy corresponds to the position of the $S_0 \rightarrow S_4$ transition (370 nm for SD #2243 and 380 nm for PD #2093) and parallel orientation of the dipole moment to that of the $S_0 \rightarrow S_2$ transition. Using the same logic, we can point to the position of the next $S_0 \rightarrow S_5$ transition (308 nm for SD #2243 and 320 nm for PD #2093) and the orientation of its dipole moment (parallel to $S_0 \rightarrow S_1$ and $S_0 \rightarrow S_3$). For comparison, the absorbance is plotted together with the anisotropy in Fig. 5. There is some correlation between the position of the $S_0 \rightarrow S_i$ transitions found from the anisotropy excitation spectrum and the position of the short wavelength absorption bands for PD #2093. For SD #2243, this correlation is less obvious because of the greater overlap of the short wavelength bands.

The next step of our investigation was to estimate the position of the $S_1 \rightarrow S_i$ ($i = 2, 3$ and higher) transitions from anisotropy measurements and quantum-chemical calculations and compare them with experimental results obtained from transient subpicosecond spectroscopy. We assumed that excited-state potential curves for the dyes under study are not shifted significantly along the nuclear coordinate axis with respect to the ground-state curves. The reasons for such an assumption are the following. First, the Stokes shift between the absorption and emission spectra is relatively small, indicating the absence of photophysical and photochemical processes leading to deformation of the excited-state potential curve. Second, a relatively small change in the dipole moments of dye molecules upon excitation testifies to the fact that the solvent relaxation cannot

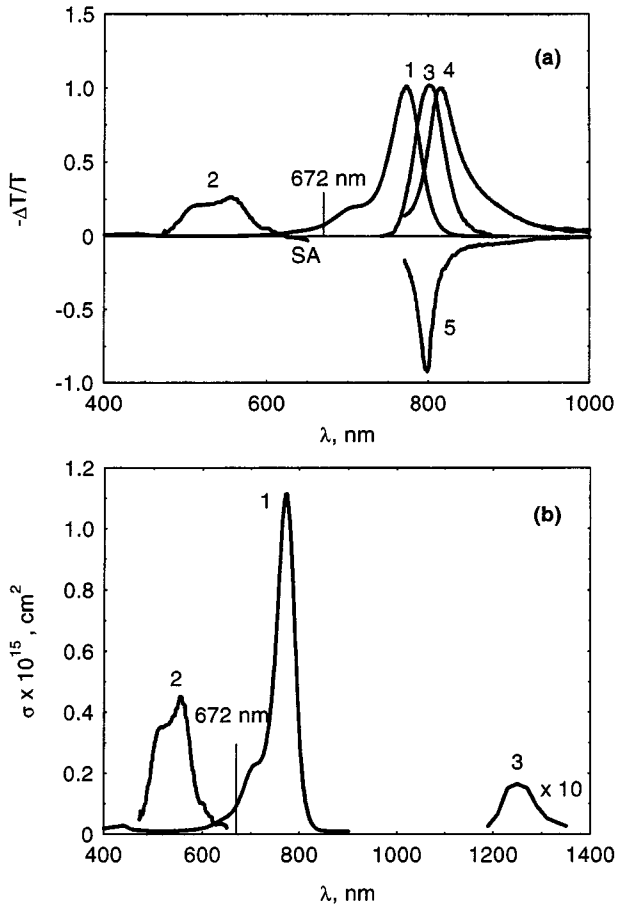

Fig. 6. (a) Transient absorption measurements for PD #2093 in ethanol. Linear absorption (1), ESA spectrum $S_1 \rightarrow S_5$ (2), fluorescence spectra, without reabsorption (3) and with reabsorption (4), and gain (5). (b) Absorption cross-section spectra $S_0 \rightarrow S_1$ (1), $S_1 \rightarrow S_5$ (2) and $S_1 \rightarrow S_2$ (3, increased ten times).

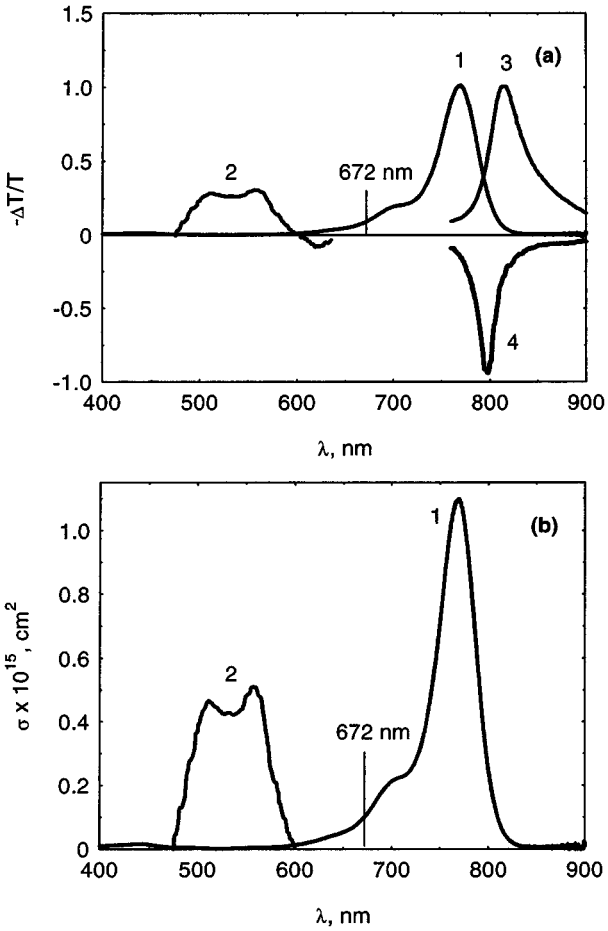

Fig. 7. (a) Transient absorption measurements for PD #2303 in ethanol. Linear absorption (1), ESA spectrum $S_1 \rightarrow S_5$ (2), fluorescence spectra with reabsorption (3) and gain (4). (b) Absorption cross-section spectra $S_0 \rightarrow S_1$ (1) and $S_1 \rightarrow S_5$ (2).

significantly shift the position of the excited-state absorption. Our experiments show that this rough approximation works well enough for prediction of the positions of the $S_1 \rightarrow S_i$ transitions, which are estimated from the difference between the $S_0 \rightarrow S_i$ and $S_0 \rightarrow S_1$ transitions. This yields the following conclusions concerning the identification of the levels and their relative positions in energy.

1) For PD #2093: 770 nm ($S_0 \rightarrow S_1$); 1270 nm ($S_1 \rightarrow S_2$); 950 nm ($S_1 \rightarrow S_3$); 750 nm ($S_1 \rightarrow S_4$); and 550 nm ($S_1 \rightarrow S_5$).
2) For SD #2243: 663 nm ($S_0 \rightarrow S_1$); 1450 nm ($S_1 \rightarrow S_2$); 1150 nm ($S_1 \rightarrow S_3$); 840 nm ($S_1 \rightarrow S_4$); and 575 nm ($S_1 \rightarrow S_5$).

From these calculations, it follows that the absorption in the visible region, which is usually utilized in optical limiting experiments at 532-nm excitation, corresponds to the $S_1 \rightarrow S_5$ transition for both PD #2093 and SD #2243. The $S_1 \rightarrow S_2$ transitions for both dyes are in the near-IR region ($\lambda > 1000$ nm). It should be mentioned that we could not obtain information about the intensities of these transitions from linear absorption spectroscopy and anisotropy measurements.

2) Excited-State Absorption Spectra: The main experimental results are presented in Figs. 6(a)–9(a). Experimental values are expressed in terms of the differential probe transmission change

$$-\Delta T/T_L = \frac{T_L - T_{\rm NL}}{T_L} = 1 - \frac{T_{\rm NL}}{T_L} \qquad (2)$$

where T_L and $T_{\rm NL}$ are the linear and nonlinear transmittance, respectively.

For all dyes, we observed a strong and broadband ESA in the visible region of the spectrum with peak positions around 550–560 nm. The FWHM for ESA in the visible region differs for each dye: 2500 cm^{-1} for PD #2098; 2900 cm^{-1} for PD #2093; 3200 cm^{-1} for PD #2303; and the broadest, 5300 cm^{-1} for SD #2243 (the FWHM for the $S_0 \rightarrow S_1$ transition in this dye is the smallest, 650 cm^{-1}). It is interesting that these bands are characterized by a more complicated vibrational structure compared to the structure of the main absorption bands. From decay kinetics measurements (up to 100 ps) performed on different wavelengths within the visible ESA spectra, we concluded that the whole band decays at approximately the same rate and therefore corresponds to a single transition. Excitation with different pump and probe polarizations indicates that the dipole moment of this transition is oriented parallel to the dipole responsible for the $S_0 \rightarrow S_1$ transition. This observation was made for all dyes studied.

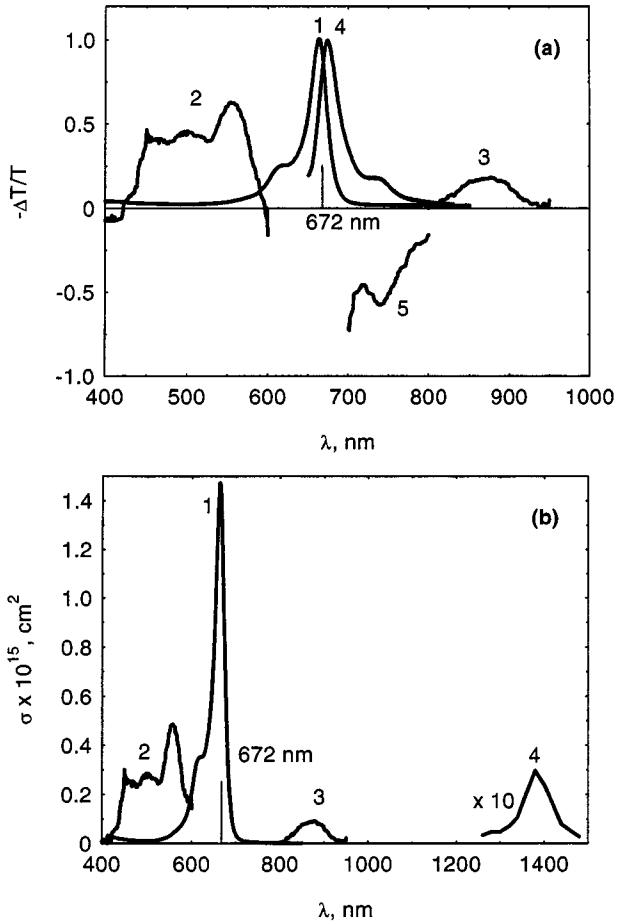

Fig. 9. (a) Transient absorption measurements for SD #2243 in ethanol. Linear absorption (1), ESA spectra $S_1 \rightarrow S_5$ (2) and $S_1 \rightarrow S_4$ (3), fluorescence spectrum without reabsorption (4), and gain (5). (b) Absorption cross-section spectra $S_0 \rightarrow S_1$ (1), $S_1 \rightarrow S_5$ (2), $S_1 \rightarrow S_4$ (3) and $S_1 \rightarrow S_2$ (4, increased ten times).

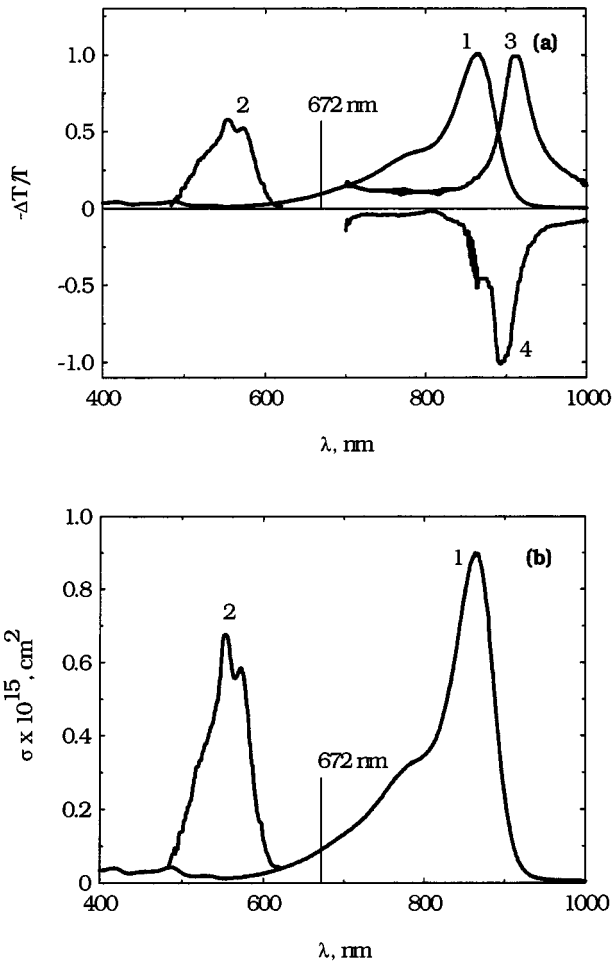

Fig. 8. (a) Transient absorption measurements for PD #2098 in ethanol. Linear absorption (1), ESA spectrum $S_1 \rightarrow S_5$ (2), fluorescence spectra with reabsorption (3), and gain (4). (b) Absorption cross-section spectra $S_0 \rightarrow S_1$ (1) and $S_1 \rightarrow S_5$ (2).

The second common feature for all these dyes is the existence of a strong gain band on the red side of the linear absorption band. For comparison of the gain band position with the emission contour, the normalized linear absorption and fluorescence bands are plotted in Figs. 6(b)–9(b). Fluorescence measurements in low concentration dye solutions ($\sim 10^{-6}$ M/l) to avoid reabsorption were performed for PD #2093 [Fig. 6(a), curve 3] and SD #2243 [Fig. 9(a), curve 4] as mentioned in Section III-A-2. The fluorescence spectra for PD #2093 [Fig. 6(a), curve 4], PD #2303 [Fig. 7(a), curve 3], and PD #2098 [Fig. 8(a), curve 3] were measured as mentioned in Section III-A3. Because of the relatively large optical density, they are shifted to the red due to reabsorption of the emission. For PD #2093 in Fig. 6(a), we show for comparison both fluorescence bands (red-shifted due to reabsorption, curve 4, and the spectrum without reabsorption, curve 3). As can be seen from the figures, the maxima of the gain bands are "blue"-shifted by about 10–15 nm from the maxima of the fluorescence bands without reabsorption. Due to the closeness of the 672-nm pumping wavelength to the fluorescence maximum in SD #2243, we could observe only the red end of the gain spectrum. This spectrum shows a peak corresponding to vibrational structure in fluorescence band. For this dye, we also observed weak saturable absorption in the region 400–420 nm, which may be attributed to absorption from S_0 to state S_3 (see Section III-B1), provided $\sigma_{03} \gg \sigma_{1i}$.

The excited-state absorption for PD #2093 and SD #2243 was studied in more detail than for all the others. For these dyes, we found additional ESA bands in the IR. To our knowledge, this is the first prediction from quantum-chemical calculations and experimental observation of these bands. For SD #2243, we found two IR ESA bands [see Fig. 9(b)], the first of which has an absorption maximum around 870 nm with FWHM $= 1000$ cm^{-1}. This is very close to the 840-nm value predicted in Section III-B1 for the $S_1 \rightarrow S_4$ transition for this dye. The maximum of the second additional ESA band (FWHM $= 500$ cm^{-1}) is observed at 1380 nm, which is in a good agreement with the predicted position of 1450 nm for the $S_1 \rightarrow S_2$ transition. Polarization decay measurements show that these transitions are oriented in the same direction as the dipole involved in ESA in the visible region. As shown in Fig. 6(b), for PD #2093, we found an IR ESA band peaked around 1250 nm, as predicted in Section III-B1 for the $S_1 \rightarrow S_2$ transition. Polarization decay measurements show that this transition is also oriented in the same direction as that for the visible ESA. The $S_1 \rightarrow S_3$ transition was not observed for either molecule, in accord with the

TABLE I
ABSORPTION CROSS-SECTIONS AT THE MAXIMUM OF $S_0 \rightarrow S_1$ AND $S_1 \rightarrow S_i$ TRANSITIONS, AND EXCITED-STATE CROSS-SECTIONS AT 532 NM. THE ERROR BARS WERE ESTIMATED AS 10% FOR ABSORPTION CROSS-SECTIONS AT THE MAXIMUM OF $S_0 \rightarrow S_1$ AND 20% FOR $S_1 \rightarrow S_i$ TRANSITIONS

Dye	Transition	Wavelength, nm	$\sigma \times 10^{16}$, cm^2
PD #2093	$S_0 \rightarrow S_1$	770	11
	$S_1 \rightarrow S_5$	532	3.0
	$S_1 \rightarrow S_5$	555	4.5
	$S_1 \rightarrow S_2$	1250	0.17
PD #2303	$S_0 \rightarrow S_1$	768	11
	$S_1 \rightarrow S_5$	532	4.3
	$S_1 \rightarrow S_5$	557	5.0
PD #2098	$S_0 \rightarrow S_1$	864	8.8
	$S_1 \rightarrow S_5$	532	3.8
	$S_1 \rightarrow S_5$	553	7
SD #2243	$S_0 \rightarrow S_1$	663	15
	$S_1 \rightarrow S_5$	532	2.5
	$S_1 \rightarrow S_5$	556	4.9
	$S_1 \rightarrow S_4$	870	0.9
	$S_1 \rightarrow S_2$	1380	0.3

quantum-chemical prediction that this transition should be forbidden by symmetry rules.

IV. DISCUSSION

A. Excited-State Cross-Section Spectra

In (2), the linear transmittance T_L and nonlinear transmittance $T_{\rm NL}$ can be written as

$$T_L(\lambda) = \exp\{-\sigma_{01}(\lambda)NL\}$$
$$T_{\rm NL}(\lambda) = \exp\{-[\sigma_{01}(\lambda)N_0 + \sigma_{1i}(\lambda)N_1 - \sigma_{10}(\lambda)N_1]L\} \quad (3)$$

where L is the optical path length in the medium; N is the total molecular concentration, which equals the sum of concentrations of the molecules in the ground (N_0) and the first excited state (N_1) in the approximation such that we can neglect the populations of any other levels; and $\sigma_{10}(\lambda)$ is a stimulated emission cross-section. Note that because absorption and emission usually involve different states in the band, $\sigma_{10}(\lambda)$ is not equal to $\sigma_{01}(\lambda)$. Hence $-\Delta T/T$ becomes

$$-\Delta T/T(\lambda) = 1 - \exp\{-[-\sigma_{01}(\lambda) + \sigma_{1i}(\lambda) - \sigma_{10}(\lambda)]N_1L\}. \quad (4)$$

Let us make some approximations. For the determination of ESA spectra in the visible region (far from the region of fluorescence emission), we can neglect $\sigma_{10}(\lambda)$. For analysis of ESA spectra in the near-IR region (870, 1250, and 1380 nm), we can neglect both $\sigma_{10}(\lambda)$ and $\sigma_{01}(\lambda)$. According to [8], the gain cross-section $\sigma_{\rm gain}(\lambda) = \sigma_{1i}(\lambda) - \sigma_{10}(\lambda)$. Analysis of ESA spectra in the region of $S_0 \rightarrow S_1$ absorption and $S_1 \rightarrow S_0$ emission is more complicated. It is seen from (4) that the position of the function $-\Delta T/T$ should depend on $\sigma_{01}(\lambda)$, $\sigma_{10}(\lambda)$, and $\sigma_{1i}(\lambda)$. In the case of $\sigma_{1i}(\lambda) \ll \sigma_{01}(\lambda)$—that is, no significant excited-state absorption in this region (like for SD #2243), $\sigma_{\rm gain}(\lambda) = -\sigma_{10}(\lambda)$ and in (4)—we can consider the sum of ground-state absorption and stimulated emission cross-sections only. In this case, the Stokes shift between absorption and fluorescence spectra determines the maximum of $-\Delta T/T$. If the Stokes shift is large (small overlapping of the bands), the function $-\Delta T/T$ may consists of two maxima corresponding to absorption and emission peaks. If the Stokes shift is small enough (large overlapping of the bands), the function $-\Delta T/T$ has only one maximum that is slightly shifted to the "blue" region compared with the fluorescence peak, i.e., closer to the crossing point of the absorption and emission spectra (0–0 transition region). From quantum-chemical calculations and analysis of $S_0 \rightarrow S_i$ spectra, we can conclude that for most PDs, the $S_0 \rightarrow S_4$ excited-state absorption should be positioned inside the linear absorption contour. The experimental data shown in Figs. 6(a)–7(a) are in agreement with this statement. They show a strong decrease of the function $-\Delta T/T$ in the region close to the maximum of the linear absorption, which is probably connected with the existence of the $S_1 \rightarrow S_i$ absorption.

To obtain an absolute determination of $\sigma_{1i}(\lambda)$ in the visible region, we used data from independent Z-scan measurements at 532 nm, which yielded σ_{1i} at 532 nm for all dyes. We then normalized $\sigma_{1i}(\lambda)$ to the 532-nm value as follows:

$$\sigma_{1i}(\lambda) = \sigma_{01}(\lambda) - \left\{[\sigma_{01}(532\,\text{nm}) - \sigma_{1i}(532\,\text{nm})] \cdot \frac{\ln(\Delta T/T)(\lambda)}{\ln(\Delta T/T)(532\,\text{nm})}\right\}. \quad (5)$$

The transient cross-section spectra for all dyes obtained by the above method are presented in Figs. 6(b)–9(b). It should be noted that all dyes are characterized by very large excited-state absorption cross-sections in the visible region, among the largest described in the literature [8], [9]. The values of these cross-sections at the maximum of each band are given in Table I.

From Table I, we can draw the following conclusions.

1) The largest excited-state absorption cross-section (7×10^{-16} cm^2) is found for PD #2098 with the longest polymethine chromophore. We do not have enough information to find a direct relationship between σ_{15} and the

TABLE II
CALCULATED AND EXPERIMENTAL CHARACTERISTICS OF $S_0 \rightarrow S_i$ ($\lambda^{max} \pm 5$ NM) AND $S_1 \rightarrow S_i$ ($\lambda^{max} \pm 15$ NM) ELECTRON TRANSITIONS

Dye	Transition	AM1 method λ^{max}, nm	Oscillator strength	PPP method λ^{max}, nm	Experiment λ^{max}, nm
SD #2243	$S_0 \rightarrow S_1$	651	1.7	648	663*
	$S_0 \rightarrow S_2$	430	0.0	436	455*
	$S_0 \rightarrow S_3$	375	0.0	384	420*
	$S_0 \rightarrow S_4$	364	0.07	354	370*
	$S_0 \rightarrow S_5$	348	0.06	350	308*
	$S_1 \rightarrow S_2$	1272	-	1336	1450*(1380**)
	$S_1 \rightarrow S_3$	888	-	940	1150*
	$S_1 \rightarrow S_4$	828	-	783	840* (870**)
	$S_1 \rightarrow S_5$	748	-	760	575* (556**)
PD #2093	$S_0 \rightarrow S_1$	653	1.819	753	770*
	$S_0 \rightarrow S_2$	386	0.007	484	480*
	$S_0 \rightarrow S_3$	315	0.144	413	430*
	$S_0 \rightarrow S_4$	297	0.107	407	380*
	$S_0 \rightarrow S_5$	263	0.002	332	320*
	$S_1 \rightarrow S_2$	942	-	1356	1270*(1250**)
	$S_1 \rightarrow S_3$	608	-	914	970*
	$S_1 \rightarrow S_4$	544	-	884	750*
	$S_1 \rightarrow S_5$	440	-	594	550* (555**)

* from absorption and anisotropy excitation measurements.
** from subpicosecond transient absorption measurements.

length of this conjugated system. This point requires further study. For this dye, σ_{15}(532 nm) is only 1.3 times less than in the peak of the linear absorption band.

2) σ_{15}(555 nm) Z for PD #2093 and σ_{15}(557 nm) for PD #2303 are about two times less than the peak value for the main linear absorption band. The physical limit of the molecular absorption cross-section probably corresponds to the value of σ_{01} at the maximum of the band. As is well known (for example, [1] and [13]) $S_0 \rightarrow S_1$ electronic transition is connected with the transit of the π-electron density from the carbon atoms in the odd position of the polymethine chain to the atoms in the even position. Due to their closeness, the overlap of their electron wave functions is the largest, leading to the largest intensity for the $S_0 \rightarrow S_1$ transition compared to other $S_0 \rightarrow S_i$ and $S_1 \rightarrow S_i$ transitions. Thus, this potential limit for the strength of the $S_1 \rightarrow S_i$ transitions for the dyes studied here has not been reached. Future experimental work should be directed at additional improvement of the molecular structure to provide a twofold increase in the ESA in the visible region. Additional ESA in the IR region (1250 nm) for PD #2093 is about 30 times less than for the ESA in the visible.
3) σ_{15}(556 nm) for SD #2243 is about three times less than at the peak of the main absorption band. It should be mentioned that this dye is characterized by the largest σ_{01} value. Additional ESA maxima in the IR region are about 5 times less for 870 nm and 17 times less for 1380 nm as compared to ESA in the visible.

ESA measurements performed for these dyes in the PUA matrix show essentially the same features found for the dyes in ethanol solutions. The only difference is the much slower rate of ESA decay kinetics. The results of decay kinetics measurements are the subject of our ongoing investigations.

The next step of our analysis is to examine the nature of possible transitions in PDs and SDs and their connection with the molecular structure.

B. Nature of the $S_0 \rightarrow S_i$ Electronic Transitions

The results of quantum-chemical calculations of the positions of electron transitions $S_0 \rightarrow S_i$ and $S_1 \rightarrow S_i$ and the experimental data obtained from anisotropy excitation and nonlinear absorption spectra are presented in Table II. Both quantum-chemical methods, AM1 and PPP, give results that are in a comparatively good agreement with the experimental data for SD #2243, while for PD #2093, the PPP method provides much better agreement with the experiment than AM1. The oscillator strengths predicted by AM1 for the higher transitions are very small, in qualitative agreement with the low experimental intensities in the region from 300 to 600 nm, in contrast to the very intense main absorption band.

The absorption bands in the visible and near-IR regions of PDs and SDs are known to be caused by π-electron transitions from the ground state to one of the excited states [1]. In the one-electron Hartree–Fock approximation, the many-electron wave function of the pth state can be written as an antisymmetric product (Slater's determinant) of one-electron wave functions, the so-called molecular orbitals (MOs). Each state corresponds to a certain electronic configuration Φ_p. These electron configurations for SD #2243 and PD #2093 are presented in Fig. 10. The ground state Φ_0 can be written as a configuration with all double occupied MOs (or molecular energetic levels), while the

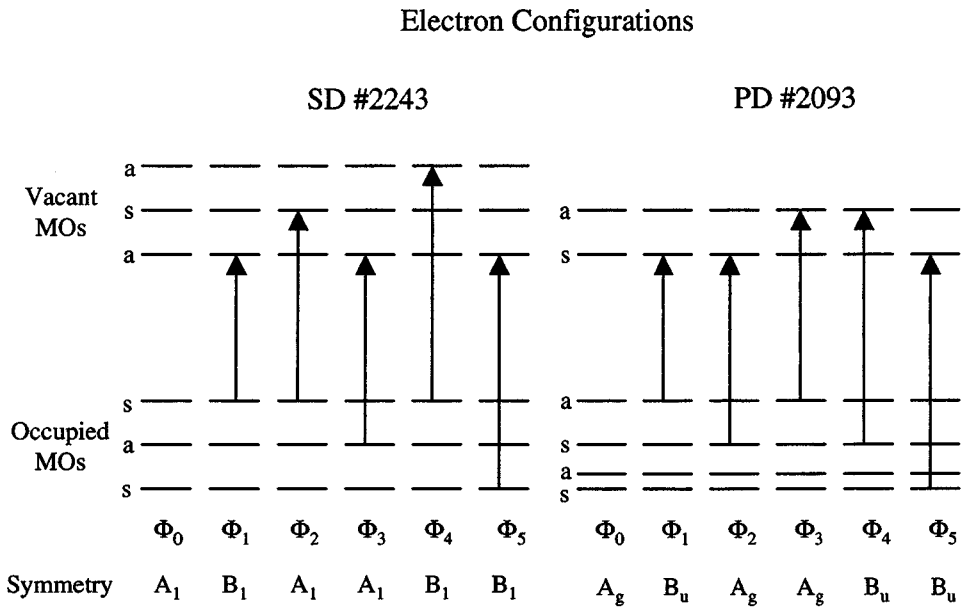

Fig. 10. Schematic diagram of electron configurations for SD #2243 and PD #2093 given in the order of the increase of their energies. The difference in configurations is connected with different topology of dyes.

excited states are presented by the electron configurations with two single occupied levels.

The next step in improving the excited-state wave functions is to take into consideration the configurational interaction. Then the wave function of the Si-state, $|\mathrm{Si}>$, can be written as the linear combination of configurations, $|\mathrm{Si}> = \Sigma T_{ip}|\Phi_p>$, where coefficient T_{ip} determines the contribution of configuration p to state i. In our calculations, we use only single excited electronic configurations. In the PPP approximation, the acceptable energies of the two to three lowest excited states were obtained with 50–60 single excited configurations. For higher transitions, the agreement with experimental data is worse than for lower transitions. This is a known limitation of the standard PPP method [13], [17].

The degree of configurational interaction depends on the overlap of the MOs and is the largest if the MOs are placed in the same part of the molecule. Fig. 11 presents the highest occupied MO (HOMO) and the lowest unoccupied MO (LUMO) as well as the nearest MOs (from HOMO -2 to LUMO $+2$) for SD #2243 and PD #2093. Calculations were made in the AM1 approximations. It is seen that HOMO and LUMO are mainly localized on the polymethine chromophore for both dyes. The next vacant MOs (LUMO $+1$ and LUMO $+2$) for SD #2243 are predominantly localized on the atoms of terminal groups. For PD #2093, the next vacant MO (LUMO $+1$) is characterized by localization of charge on the polymethine chromophore with slight involvement of the terminal groups. For LUMO $+2$, the localization on the phenyl substituent plays the most significant role in the electronic transition. As can be seen, LUMO $+1$ and LUMO $+2$ are very different for SD #2243 compared to PD #2093. The occupied MOs (HOMO -1 and HOMO -2) for both dyes are distributed over the whole dye structure.

The PPP calculation shows that the $S_0 \rightarrow S_1$ transition can be represented mainly by the electronic configuration Φ_1 with two single occupied MOs corresponding to HOMO and LUMO in the ground state (Φ_0 configuration), so that the wave function $|S_1> \approx 0.98|\Phi_1>$ for SD #2243 and $|S_1> \approx 0.97|\Phi_1> - 0.23|\Phi_4>$ for PD #2093. These $S_0 \rightarrow S_1$ transitions occur between states of different symmetry and are therefore allowed, leading to the high intensity of the main absorption bands. The transition moment is directed along the polymethine chain (between two nitrogen atoms in the terminal groups).

The higher electronic transitions $S_0 \rightarrow S_2$ involve the deeper occupied levels and the next vacant MOs. Expansion of the PPP calculations on the second excited state gives the following values of wave functions: $|S_2> \approx 0.99|\Phi_2>$ for SD #2243 and $|S_2> \approx 0.91|\Phi_2> - 0.23|\Phi_3>$ for PD #2093. Thus the S_2-state in the squarylium dye is practically "pure" and in PD #2093 is mixed with a portion of the higher configuration. Because of configurational interactions, this mixing leads to an additional decrease in $S_0 \rightarrow S_2$ transition energy.

$S_0 \rightarrow S_2$ is the transition between states of the same symmetry and hence is forbidden (within the accuracy of the calculation). The dipole moment of this transition is directed perpendicular to the main chromophore (polymethine chain). The PPP calculation with a comparatively small number of configurations gives the result that the third excited state S_3 in both dyes should have the same symmetry as that of S_2 (A_1 and A_g; see Fig. 10). This result does not agree with the experimental anisotropy excitation measurements showing that the $S_0 \rightarrow S_3$ transition is polarized almost parallel to the $S_0 \rightarrow S_1$ transition and hence is of $B_1(B_u)$ symmetry. This is an indication that a larger configurational interaction (or a larger number of configurations) has to be used. A new calculation with a considerable increase in the number of configurations leads to an inversion of the symmetry of the calculated S_3 and S_4 states. Hence the lowest of the states of symmetry $B_1(B_u)$ that are split by the configurational interection is found to be situated lower than the next state of symmetry $A_1(A_g)$. Calculations show that the

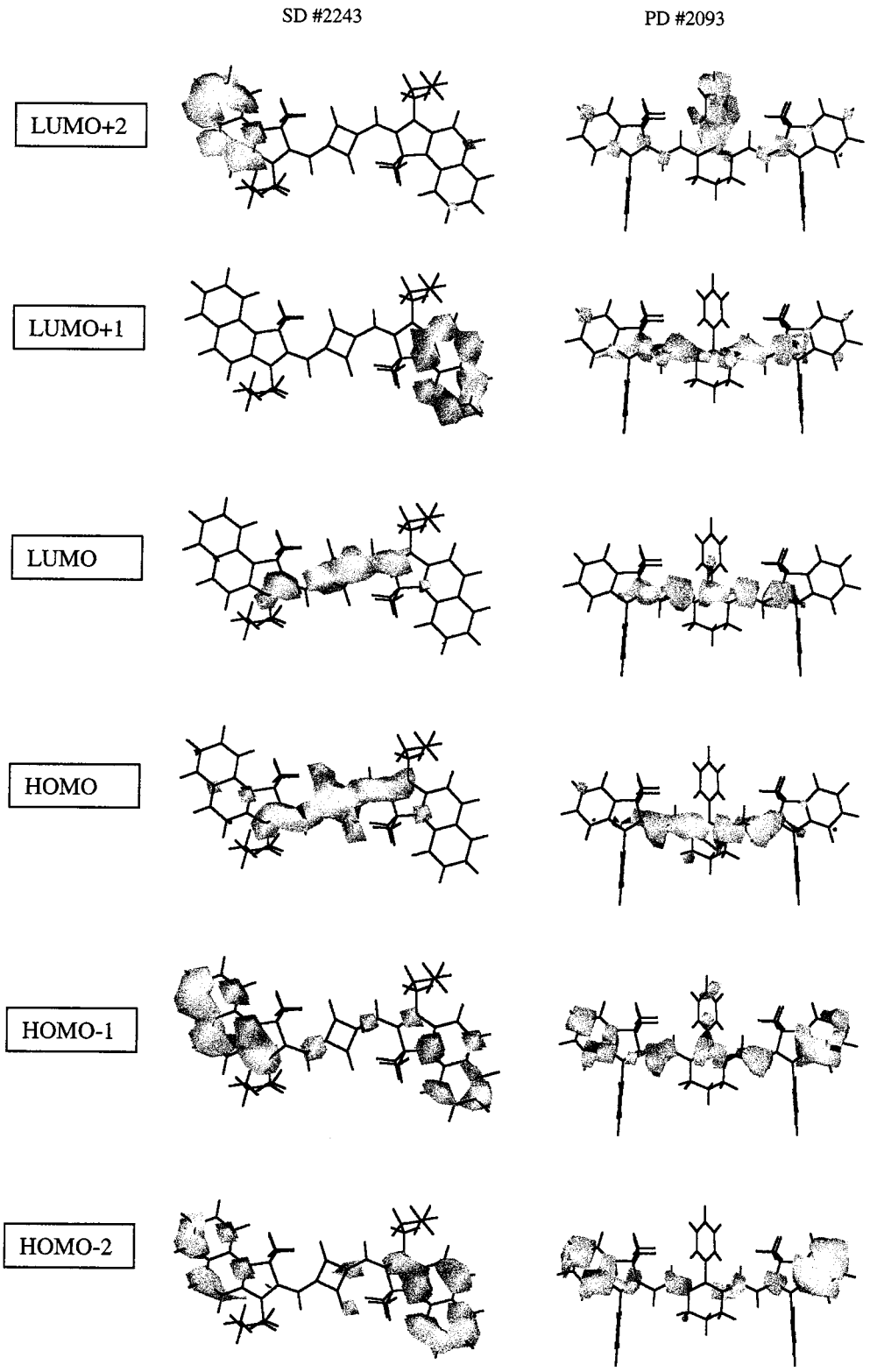

Fig. 11. Localization of molecular orbitals from HOMO -2 to LUMO $+2$ for SD #2243 and PD #2093 calculated in AM1 approximation.

energies of the next transitions, $S_0 \rightarrow S_4$ and $S_0 \rightarrow S_5$, and higher are relatively close. The order of their displacement and symmetry depends on the number of configurations involved into calculations. In addition, for the higher electronic states, the "pure" symmetric configuration cannot be achieved and the symmetry selection rules become less strict. Therefore, the role of the experimental investigation (especially anisotropy excitation measurements) for higher transitions is extremely important to check the quantum-chemical calculations. The molecular geometry and charge distribution obtained for SD #2243 using the AM1 method are similar to the results obtained from the CNDO/2 method performed in [18].

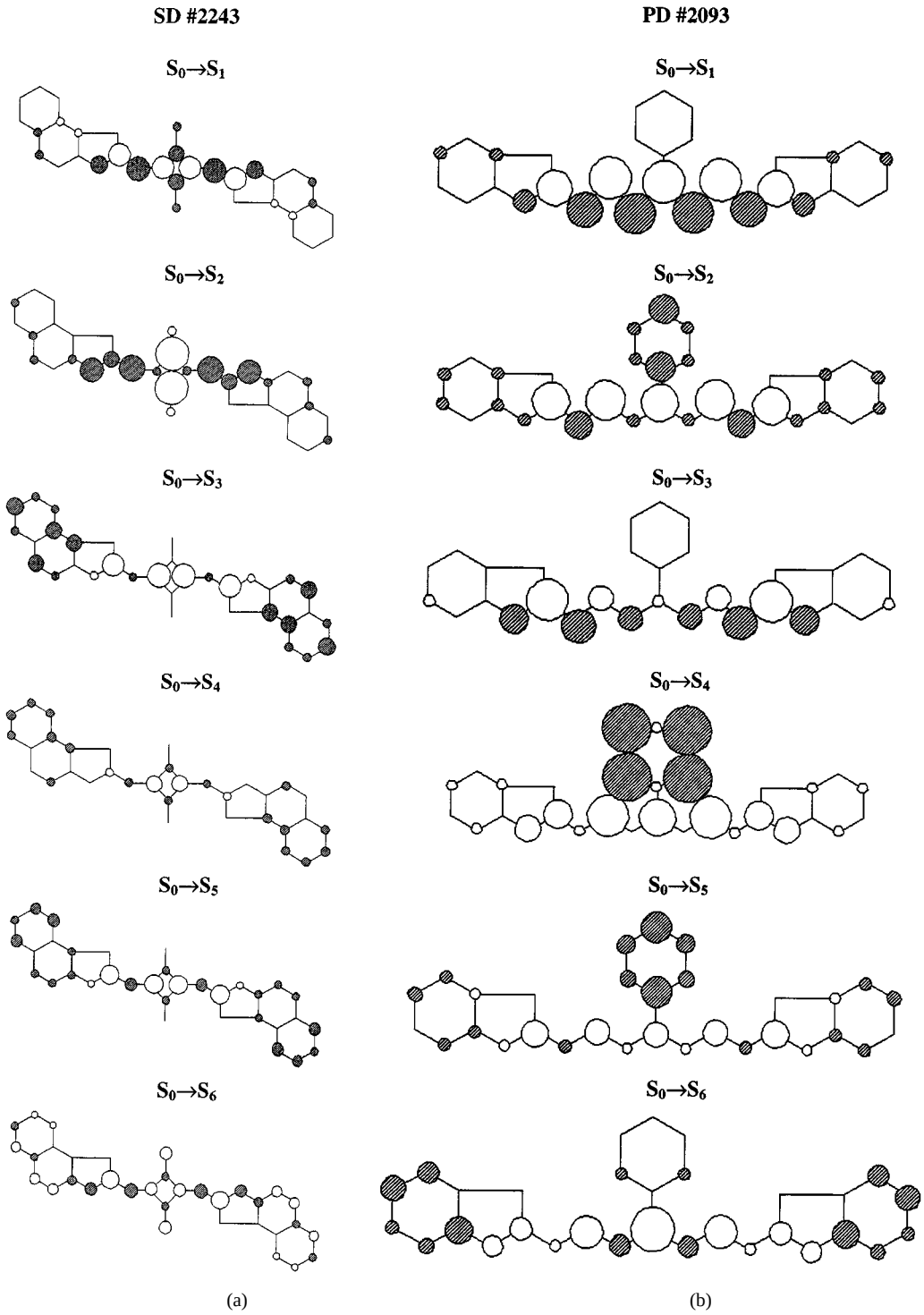

Fig. 12. Electron energy redistribution on transitions $S_0 \rightarrow S_i$ for (a) SD #2243 and (b) PD #2093. Dark circles correspond to a decrease of electron density due to a transition, while the white circles correspond to an increase. The diameters of the circles approximately reflect the values of electron density change.

Schematic diagrams of the electron density redistribution upon transitions $S_0 \rightarrow S_i$, calculated as the difference between charge distribution in the final and initial states, are shown in Fig. 12. It is seen that the first transition $S_0 \rightarrow S_1$ is accompanied by the transit of the π-electron density from the carbon atoms in the odd positions of the polymethine chain to the atoms in the even positions, that is, a polymethine electronic transition (PET) [17]. Despite the chain branching in SD #2243 and large charge density on the carbon atoms in the "square" cycle, the nature of the first electronic transition is the same as in any standard polymethine dye, for example, in PD #2093. However, the nature of the higher transitions in PD #2093 and SD #2243 is different. It is seen from Fig. 12(b) that the $S_0 \rightarrow S_2$ transition for PD #2093 is connected with the electron density transfer from the atoms of the phenyl substituent to carbon atoms in the even positions of the polymethine chain.

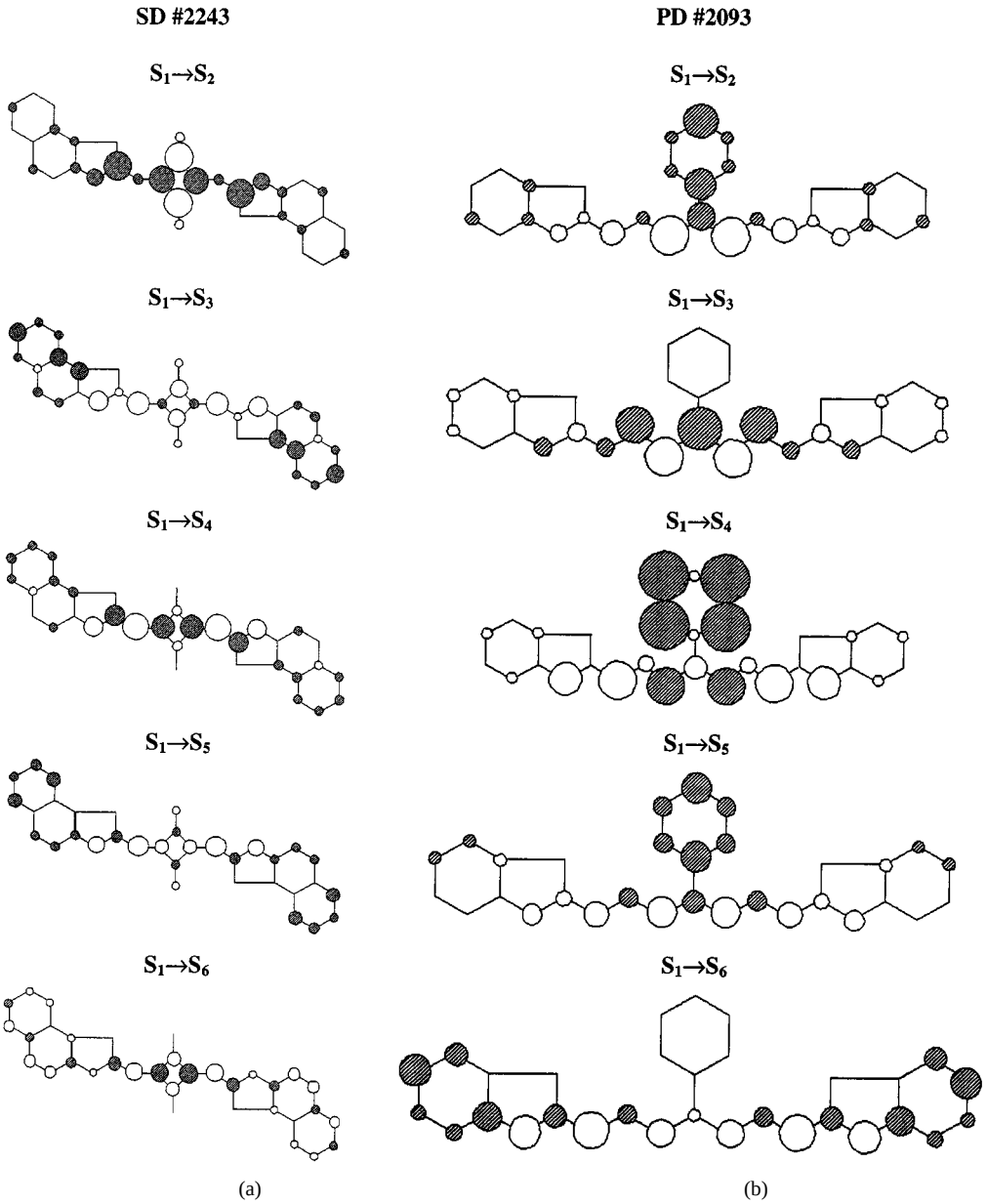

Fig. 13. Electron energy redistribution on transitions $S_1 \rightarrow S_i$ for (a) SD #2243 and (b) PD #2093.

Total density (or charge) transfer from the phenyl fragment to the chain fragment occurs with the $S_0 \rightarrow S_4$ transition. A similar electron transition is classified as the charge transfer (CT) transition. Meanwhile, the $S_0 \rightarrow S_3$ transition is similar to the $S_0 \rightarrow S_1$, i.e., is PET, only with a rather different degree of atomic density change. The $S_0 \rightarrow S_5$ transition is connected with the electron density transfer from the polymethine chain to the phenyl substituent. The terminal groups are involved in the $S_0 \rightarrow S_6$ transition only.

In contrast, the $S_0 \rightarrow S_2$ transition in SD #2243 [Fig. 12(a)] is accompanied by the electron transfer from the chain atoms placed out of the "square" cycle to the two central carbon atoms in the "square" cycle having the large positive charge density in the ground state. The next transition, $S_0 \rightarrow S_3$, is characterized by an electron density transfer between the molecular fragments: from the terminal groups to the atoms in the main chromophore. Finally, the $S_0 \rightarrow S_4$, $S_0 \rightarrow S_5$, and $S_0 \rightarrow S_6$ transitions are a mixture or combination of PET and CT transitions but with the necessary involvement of the terminal groups.

C. Nature of the $S_1 \rightarrow S_i$ Electron Transitions

The main fundamental result obtained from the quantum-chemical calculations confirms that the energy of the $S_1 \rightarrow S_2$ should be lower than the energy of the $S_0 \rightarrow S_1$ transition. That fact was supported by calculations in other approximations (CNDO/S, MNDO [18], ZINDO/S [3]). The results calculated in the AM1 and PPP approximations, as well as the data obtained from experimental spectra, are presented in Table II.

According to symmetry selection rules, transitions restricted in the linear absorption spectra should be allowed for $S_1 \rightarrow S_i$ transitions. Therefore, the $S_1 \rightarrow S_2$ transition should be allowed and the dipole polarized parallel to that for $S_0 \rightarrow S_1$. The next transition, $S_1 \rightarrow S_3$, should be forbidden (or weakly allowed) as the transition between the states of the same symmetry

with dipole polarized perpendicular to that for the $S_0 \rightarrow S_1$ transition. Perhaps the $S_1 \rightarrow S_4$ and higher transitions are allowed because of relaxed symmetry selection rules in linear absorption. It is interesting to compare the electron density redistribution upon $S_1 \rightarrow S_i$ transitions presented in Fig. 13 with the corresponding diagram for the $S_0 \rightarrow S_i$ transitions (Fig. 12). The $S_1 \rightarrow S_2$, $S_1 \rightarrow S_4$, and $S_1 \rightarrow S_5$ transitions in PD #2093 are mainly connected with the charge transfer between the molecular fragments, while the $S_1 \rightarrow S_3$ transition is typically PET and similar to the $S_0 \rightarrow S_1$ transition. In SD #2243, the $S_1 \rightarrow S_2$, $S_1 \rightarrow S_3$, and $S_1 \rightarrow S_5$ transitions are connected with the electron density transfer between the molecular fragments. The $S_1 \rightarrow S_2$ transition is similar to the second transition from the ground state $S_0 \rightarrow S_2$, while $S_1 \rightarrow S_3$ and $S_1 \rightarrow S_5$ are accompanied by a charge transfer from the terminal groups to the chain, which is similar to $S_0 \rightarrow S_3$, and the $S_1 \rightarrow S_4$ transition is a mixture of PET and CT transitions with the involvement of the terminal groups (Fig. 13).

V. Conclusion

Nonlinear absorption pump-probe spectroscopy using a subpicosecond white-light continuum as a probe in combination with steady-state anisotropy excitation measurements and quantum-chemical modeling gives fundamental information about the nature of excited-state transitions and their relationships with molecular structure. For the first time in these types of molecules, we predicted and found additional ESA spectra in the near IR region.

Analyzing the results of quantum-chemical calculations and experimental data, we reach the following conclusions.

1) The large oscillator strength ESA spectra in the visible region (500–600 nm) for all dyes—PD #2093, PD #2303, PD #2098, and SD #2243—are connected with $S_1 \rightarrow S_5$ transitions.
2) For PD #2093, visible ESA transition is primarily connected with charge transfer between the molecular fragments, from the phenyl substituent and three central carbon atoms of the polymethine chain to the rest of the polymethine chromophore and terminal groups.
3) For SD #2243, this transition is connected with charge transfer from the terminal groups to the polymethine chromophore. It is probable that for such high transitions as $S_1 \rightarrow S_5$, there is a mixture of transitions of different nature, and therefore these transitions may be allowed. Experimental measurements show that all dipole moments of $S_1 \rightarrow S_2$, $S_1 \rightarrow S_4$, and $S_1 \rightarrow S_5$ transitions are almost parallel to each other and are oriented close to parallel to the dipole involved in the $S_0 \rightarrow S_1$ transition (Section III-B1).
4) The ESA spectrum in the region of 1250 nm for PD #2093 is connected with the $S_1 \rightarrow S_2$ transition, which is allowed and connected with charge transfer from the phenyl substituent to the polymethine chromophore. The dipole moments of the $S_1 \rightarrow S_5$ and $S_1 \rightarrow S_2$ transitions are oriented almost parallel to that for the $S_0 \rightarrow S_1$ transition. The transition $S_1 \rightarrow S_3$ (PET) is not allowed and indeed was not observed in our experiments.
5) The ESA spectrum in the region of 1380 nm for SD #2243 is connected with the $S_1 \rightarrow S_2$ transition. This transition is allowed and connected with electron transfer from the polymethine chromophore (also slightly involving the terminal groups) to two central carbon atoms in the "square" cycle. The $S_1 \rightarrow S_3$ transition is not allowed and was not observed experimentally.
6) The ESA spectrum in the region of 870 nm for SD #2243 is connected with the $S_1 \rightarrow S_4$ transition, which is allowed, primarily involving the polymethine chromophore and only slightly the terminal groups.
7) The existence of ESA inside of the linear absorption contour of PD #2093 (750–800 nm) is probably connected with the $S_1 \rightarrow S_4$ transition. This allowed transition involves charge transfer from the phenyl substituent and two central carbon atoms of the polymethine chain to the rest of the polymethine chromophore and terminal groups.

We expect that the results of this paper will stimulate the further development of methodologies of quantum-chemical calculations as well as the synthesis of new dyes with improved properties for nonlinear optical applications.

Acknowledgment

The authors would like to thank Dr. J. Gallay and Dr. M. Vincent (LURE, Orsay, France) for their help in anisotropy excitation measurements of PD #2093.

References

[1] N. Tyutyulkov, J. Fabian, A. Mehlhorn, F. Dietz, and A. Tadjer, *Polymethine Dyes. Structure and Properties*. Sofia, Bulgaria: St. Kliment Ohridski Univ. Press, 1991.
[2] M. Matsuoka, Ed., *Infrared Absorbing Dyes*. New York: Plenum, 1990, pp. 7–33.
[3] W. M. F. Fabian and J. M. Kauffman, "Computational methods as an aid in the design of fluorophores with predictable absorption and emission wavelengths," *J. Luminescence*, vol. 85, no. 1–3, pp. 137–148, 1999.
[4] J. Rodrigues, D. Scherlis, D. Estrin, P. F. Aramendia, and R. M. Negri, "AM1 study of the ground and excited state potential energy surfaces of symmetric carbocyanines," *J. Phys. Chem. A*, vol. 101, no. 35, pp. 6998–7006, 1997.
[5] F. Momicchioli, I. Baraldi, and G. Berthier, "Theoretical-study of trans-cis photoisomerism in polymethine cyanines," *Chem. Phys.*, vol. 123, no. 1, pp. 103–112, 1988.
[6] F. Meyers, S. R. Marder, and J. W. Perry, *Chemistry of Advanced Materials: An Overview*, L. V. Interrante and M. J. Hampden-Smith, Eds. New York: Wiley-VCH, 1998, pp. 207–269.
[7] M. Pittman, P. Plaza, M. M. Martin, and Y. H. Meyer, "Subpicosecond reverse saturable absorption in organic and organometallic solutions," *Opt. Commun.*, vol. 158, no. 1–6, pp. 201–212, 1998.
[8] Y. H. Meyer, M. Pittman, and P. Plaza, "Transient absorption of symmetrical carbocyanines," *J. Photochem. Photobiol. A: Chem.*, vol. 114, no. 1, pp. 1–21, 1998.
[9] J. H. Lim, O. V. Przhonska, S. Khodja, S. Yang, T. S. Ross, D. J. Hagan, E. W. Van Stryland, M. V. Bondar, and Y. L. Slominsky, "Polymethine and squarylium molecules with large excited-state absorption," *Chem. Phys.*, vol. 245, no. 1–3, pp. 79–97, 1999.
[10] E. W. Van Stryland, D. J. Hagan, T. Xia, and A. A. Said, *Nonlinear Optics of Organic Molecules and Polymers*, H. S. Nalva and S. Miyata, Eds. New York: CRC, 1997, pp. 841–860.
[11] O. V. Przhonska, J. H. Lim, D. J. Hagan, E. W. Van Stryland, M. V. Bondar, and Y. L. Slominsky, "Nonlinear light absorption of polymethine dyes in liquid and solid media," *J. Opt. Soc. Amer. B*, vol. 15, no. 2, pp. 802–809, 1998.
[12] J. Fabian and R. Zahradnic, *Wis. Z. Techn. Univ. Dresden*, vol. 26, pp. 315–323, 1977.

[13] A. D. Kachkovskii, "The nature of electronic transitions in linear conjugated systems," *Russian Chem. Rev.*, vol. 66, no. 8, pp. 647–664, 1997.
[14] J. R. Lakowicz, *Principles of Fluorescence Spectroscopy*, 2nd ed. Norwell, MA: Kluwer Academic/Plenum, 1999.
[15] R. L. Fork, C. V. Shank, C. Hirlimann, R. Yen, and W. J. Tomlinson, "Femtosecond white-light continuum pulses," *Opt. Lett.*, vol. 8, no. 1, pp. 1–4, 1983.
[16] F. E. Hernandez and D. J. Hagan, "Continuously-variable wavelength independent polarization rotator," U. S. Patent, 2001.
[17] A. D. Kachkovski, "Electronic properties of polymethine systems. 3. Polymethine and quasilocal electron transitions," *Dyes Pigments*, vol. 24, pp. 171–183, 1994.
[18] R. W. Bigelow and H. J. Freund, "An MNDO and CNDO/S(S + DES CI) study on the structural and electronic properties of a model squaraine dye and related cyanine," *Chem. Phys.*, vol. 107, no. 2–3, pp. 159–174, 1986.

Raluca A. Negres, photograph and biography not available at the time of publication.

Olga V. Przhonska, photograph and biography not available at the time of publication.

David J. Hagan (M'87–SM'99) received the Ph.D. degree from Heriot-Watt University, U.K., in 1985.

He spent two years as a Research Scientist at North Texas State University, where he performed research on self-protecting optical limiters. He joined the University of Central Florida in 1987 as a Founding Member of the Center for Research and Education in Optics and Lasers (CREOL) faculty. Since then, he has conducted research on optical limiting devices, fundamental mechanisms for nonlinear absorption and refraction in semiconductors and dielectrics, and cascaded second-order nonlinearities for optical switching devices. More recently, he has been studying nonlinear processes in organics. Since 1991, he has run the School of Optics/CREOL Summer Research Experiences for Undergraduates program. He is now Associate Director for Academic Programs for the School of Optics.

Eric W. Van Stryland, photograph and biography not available at the time of publication.

Mikhail V. Bondar, photograph and biography not available at the time of publication.

Yuriy L. Slominsky, photograph and biography not available at the time of publication.

Alexei D. Kachkovski, photograph and biography not available at the time of publication.